Letter

Absolute Measurement of Pore Size based on Nonground Eigenstates in Magnetic-Resonance Relaxation

Armin Afrough,[1,2,†] Sarah Vashaee,[1] Laura Romero Zerón,[2] and Bruce Balcom[1,*]

[1] *UNB MRI Research Centre, Physics Department, University of New Brunswick, Fredericton, NB E3B 5A3, Canada*

[2] *Department of Chemical Engineering, University of New Brunswick, Fredericton, NB E3B 5A3, Canada*

(Received 1 November 2018; revised manuscript received 3 February 2019; published 23 April 2019)

Magnetization evolution due to translational motion of spins in magnetic fields is governed by the Bloch-Torrey equations. In confined geometries, magnetization of such systems is often expressed as a series of eigenstates, the eigenvalues of which are related to the characteristic confinement length. We highlight the importance of nonground eigenvalues and their contribution to the relaxation of initially homogeneous magnetization by longitudinal and transverse ^{1}H relaxation processes in porous materials. We show that a simple magnetic resonance relaxation measurement can reliably characterize confinement size in fluid-occupied porous materials. Pore sizes calculated from the eigenvalues are shown to agree with independent x-ray microtomography and electron microscopy measurements in rock samples.

DOI: 10.1103/PhysRevApplied.11.041002

Confined fluids are ubiquitous in nature and in technological materials. Water in cytosol, geological formations, soil, cement, and wood are but a few examples. Diffusion of spins in porous materials, with an eigenfunction expansion and diffusion propagator, provides information on the surface-to-volume ratio [1], pore size [2,3], periodicity [4,5], and length scales [3] of fluid confinements. The evolution of magnetization $\mathbf{M}(\mathbf{r},t)$ in a fluid with scalar self-diffusivity D is governed by the Bloch-Torrey equations [6]

$$\left(\frac{\partial}{\partial t} - D\nabla^2 + \frac{1}{T_{2b}}\right) M_+(\mathbf{r},t) = 0, \tag{1}$$

in the transverse plane, where $M_+ = M_x + iM_y$, and

$$\left(\frac{\partial}{\partial t} - D\nabla^2 + \frac{1}{T_{1b}}\right) M_z(\mathbf{r},t) = \frac{M_0}{T_{1b}}. \tag{2}$$

in the direction of the static magnetic field. In the above equations, M_0 is the equilibrium magnetization of confined fluid with bulk longitudinal and transverse relaxation time constants T_{1b} and T_{2b}, respectively. T_1 and T_2 are the exponential decay constants of M_z and M_+ to M_0 and 0, respectively.

Due to enhanced magnetization relaxation at wetted surfaces by homonuclear dipole-dipole coupling, cross relaxation by other nuclear spins, and relaxation by free electrons and paramagnetic ions [7], Eqs. (1) and (2) are subject to Fourier boundary conditions

$$(D\hat{\mathbf{n}}\cdot\boldsymbol{\nabla} + \rho_2)\, M_+(\mathbf{r},t) = 0, \tag{3}$$

and

$$(D\hat{\mathbf{n}}\cdot\boldsymbol{\nabla} + \rho_1)\, M_z(\mathbf{r},t) = 0, \tag{4}$$

where ρ_1 and ρ_2 are longitudinal and transverse surface relaxivities, respectively. In general, self-diffusivity will be a tensor and ρ_1 and ρ_2 may be heterogenous; however, they are treated as constant scalars here.

Simple magnetic resonance experiments in porous media typically commence with a homogeneous magnetization such as $M_z(\mathbf{r},t) = -M_0$ or $M_+(\mathbf{r},t) = M_0$. Previous attempts to extract the system geometry and parameters of magnetic resonance relaxation in porous media from Eqs. (1) and (2), largely the work of Y. Q. Song and coworkers [2,3], have been focused on creating an inhomogeneous magnetization by employing internal magnetic-field gradients to significantly accentuate the nonground eigenstates. Recent efforts [8–10] have been directed at diffusive coupling between different environments and have provided compelling evidence (for example, see [9], their Fig. 1) that nonground eigenstates contribute to one-dimensional (1D) and two-dimensional (2D) magnetic resonance relaxation data. Other researchers [11–13] have also recognized the contribution of nonground eigenvalues to magnetic resonance relaxation in porous media. However, these works have not fully explored the opportunities this phenomenon

*bjb@unb.ca

†Current address: Centre for Oil and Gas, Technical University of Denmark, Kgs. Lyngby 2800, Denmark

provides, for example, in characterizing complex pore geometries in natural samples.

Our objective is to clearly demonstrate that nonground eigenstates contribute to longitudinal and transverse ^{1}H magnetic resonance relaxation measurements with homogeneous magnetization in porous materials. We also show that a straightforward 2D relaxation measurement of T_1 and T_2 may be processed to yield an absolute confinement size. It is shown in this work that while the ground eigenstate dominates the diffusion of spins, it is perfectly feasible to observe nonground eigenstates with a much reduced intensity; the first, and in some cases even the second, nonground eigenvalue may be observed in relaxation data. The distinctive pattern of such eigenvalues makes it possible to recognize them in porous materials, even with multiple pore sizes.

The existence of nonground eigenstates in magnetic resonance measurements of homogeneous magnetization permits the design of alternative porous media measurement methods. These ideas will also permit reprocessing of a very large body of extant magnetic resonance measurements.

We demonstrate the importance of nonground eigenstates through two examples using the $T_1 - T_2$ relaxation correlation method. Two-dimensional magnetic resonance relaxation methods dramatically improve our understanding of complex diffusion dynamics and exchange in porous media. The $T_1 - T_2$ magnetic resonance relaxation correlation experiment [14,15] provides rich information on pore fluid dynamics. The $T_1 - T_2$ method is analyzed by 2D multi-exponential analysis [16] and can simultaneously characterize multiple eigenvalues of the system. Similar ideas may also be applied to 1D relaxation data.

Radio frequency (rf) pulses applied at the Larmor frequency $f = (\gamma/2\pi)B_0$ of ^{1}H rotates the sample magnetization vector into the transverse plane where it may be observed by inducing a voltage in the probe. The $T_1 - T_2$ method is composed of a T_1 encoding segment and a T_2 encoding segment

$$\underbrace{\left[\pi - \tau_1 - \frac{\pi}{2}\right]}_{T_1 \text{ encoding}} \underbrace{\left[-(\tau_i - \pi - \tau_i)_N\right]}_{T_2 \text{ encoding}}. \tag{5}$$

The T_1 encoding commences with a 180° pulse followed by a waiting period τ_1 and a 90° pulse. T_2 information is imparted by the second segment with 180° pulses, with a time spacing of $2\tau_i$ and a phase shift of 90° compared to other rf pulses. Spin echoes form between refocusing 180° pulses in the second segment at $\tau_2 = 2k\tau_i$ with $1 < k \leq N$, where τ_2 is the time beginning in the second segment.

By varying the τ_1 encoding period P times and keeping τ_i and N constant, the measurement of Eq. (5) acquires time-domain relaxation correlation information as a $P \times N$ matrix $m_+(\tau_1, \tau_2)$ where only spin echoes are acquired by the rf coil. The magnetization m_+ acquired by the rf coil is equal to

$$m_+(\tau_1, \tau_2) = \int_{\mathbf{r}} M_+(\mathbf{r}, \tau_1, \tau_2)\, d\mathbf{r}, \tag{6a}$$

$$= \sum_{q=0}^{\infty} \sum_{p=0}^{\infty} I(T_{1,p}, T_{2,q}) e^{-\tau_1/T_{1,p}} e^{-\tau_2/T_{2,q}}, \tag{6b}$$

where the deviation of the signal from equilibrium is normalized in the longitudinal direction. A regularized inverse 2D Fredholm integral of the first kind transforms the measured signal $m_+(\tau_1, \tau_2)$ into a 2D relaxation correlation function $I(T_{1,p}, T_{2,q})$ from which eigenvalues of magnetic resonance relaxation may be identified. We employ the inversion algorithm of [17] in this work. Increasing the regularization parameter α penalizes the complexity of the solution; therefore, large α leads to smooth solutions whereas small α leads to a discretized result [17]. Equation (6) assumes the rf coil is uniformly sensitive within the sample space.

The Damköhler number of the second kind

$$\mathrm{Da}_i^{\mathrm{II}} = \frac{\rho_i l}{D}, \tag{7}$$

represents the ratio of magnetization relaxation rate at domain boundaries to the rate of mass diffusivity in a confined geometry with characteristic length l. Equation (7) in magnetic resonance relaxation of porous materials is analogous to the Damköhler number of the second kind in chemical reaction engineering that describes the effect of surface reaction kinetics on the overall diffusion-reaction process [18]. i equals 1 or 2 for longitudinal and transverse relaxation, respectively. ρ_i is analogous to the surface reactivity and l is analogous to the diffusion length in chemical reaction engineering. $\mathrm{Da}_i^{\mathrm{II}}$ sets the diffusion or surface relaxation dependence of the relaxation time constants represented in $I(T_{1,p}, T_{2,q})$. In simple geometries, and for arbitrary $\mathrm{Da}_i^{\mathrm{II}}$ values, the eigenvalues of magnetization evolution in a confined environment are

$$T_{i,n} = \frac{l^2}{4D\,\xi_{n,i}^2}, \tag{8}$$

where $\xi_{n,i}$ are functions of confinement geometry, diffusion coefficient, eigenvalue number n, and $\mathrm{Da}_i^{\mathrm{II}}$. In a planar pore geometry, $\xi_{n,i}$ are the positive roots of

$$2\xi_{n,i} \tan \xi_{n,i} = \mathrm{Da}_i^{\mathrm{II}}. \tag{9}$$

Equations (7)–(9), adapted from the work of Brownstein and Tarr [19], are valid for planar geometries for both ground $n = 0$ and nonground $n > 0$ eigenvalues and for longitudinal $i = 1$ and transverse $i = 2$ relaxation processes. A correct combination of pore size l, longitudinal

surface relaxivity ρ_1, and transverse surface relaxivity ρ_2 leads to a cluster of eigenvalue peaks that, through the Brownstein-Tarr theory, matches experimental peak locations in $T_1 - T_2$ experiments. At $\mathrm{Da}_i^{\mathrm{II}} \to 0$ or $\mathrm{Da}_i^{\mathrm{II}} \to \infty$, the ratio of eigenvalues of the diffusion-relaxation partial differential equations is simplified. However, complete numerical solutions of Eqs. (7)–(9) should be used for predicting pore size due to their nonlinearity.

In natural porous media, pore size is a distribution and not a single number. It is common practice in applied science and engineering, however, not to use the distributions of pore size, but rather a parameter describing its central tendency. Once the mean pore size is determined, the data can likely be further processed to yield the standard deviation of pore size. The effect of pore shape does not significantly affect eigenvalues, and their intensities, of the magnetic resonance relaxation in porous media. This is especially true for $\mathrm{Da}_i^{\mathrm{II}} \ll 100$ (see [19], their Figs. 1 and 2). Diffusion relaxation in porous media is usually in the intermediate-diffusion region, where $1 < \mathrm{Da}_i^{\mathrm{II}} < 10$ and the effect of pore shape is not significant.

Two geological samples, Berea sandstone and Indiana limestone with SEM images shown in Fig. 1, with different pore geometries and constitutive minerals demonstrate the distinctive pattern of eigenvalues in simple longitudinal and transverse ^{1}H magnetic resonance relaxation measurements. We show that simple magnetic resonance relaxation measurements can measure the absolute value of the confinement size. The new confinement size measurement method is verified in three glass bead packs of different, but uniform, bead size (results not reported). In natural porous materials, this alternative method predicts correct values of pore size compared to ground truth measurements of SEM microscopy and x-ray microtomography imaging, even in the carbonate sample with a bimodal pore size distribution.

The Berea sample used in this study is an Upper Devonian sandstone from the Kipton formation, a grain-supported rock with quartz, feldspar, and micaceous clay minerals that has a porosity of 0.20. The pore size mode from microscopy is 26 μm with a pore size distribution that is log-normal.

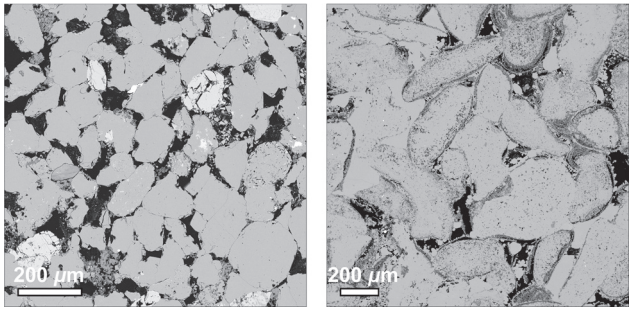

FIG. 1. Backscattered electron scanning microscopy images of resin-impregnated Berea sandstone (left) and Indiana limestone (right) with polished surfaces. Resin-filled pore space is black; in the sandstone sample, quartz is medium gray, feldspar is light gray, and clay is dark gray. Virtually all of the limestone is composed of calcite.

The Indiana limestone sample has a grain-dominated fabric, made up of fossil fragments and oolites, with calcite cement. Indiana limestone features small calcite crystals lining the pore surface and intraparticle porosity in some grains. The limestone sample features a bimodal pore size distribution in backscattered electron microscopy images with a porosity of 0.15. The large and small pore modes are 50 and 10.1 μm, respectively, both from electron microscopy.

The regularization parameter α employed in the inverse Fredholm integral transformation of the 2D relaxation correlation function $I(T_{1,p}, T_{2,q})$ can cause significant blurring of eigenvalues. However, a proper choice of the regularization parameter will demonstrate multimodal features of $I(T_{1,p}, T_{2,q})$. Such 2D relaxation correlation functions for Berea sandstone and Indiana limestone at $B_0 = 0.05$ T are shown in Fig. 2. The regularization parameter for the multiexponential analysis of relaxation measurements are varied over seven orders of magnitude, with three examples shown in Fig. 2. Eigenvalues of magnetization relaxation are labeled as *Epq*, where *E* determines the environment, and *p* and *q* are eigenstate numbers, respectively, for $T_{1,p}$ and $T_{2,q}$. *Ppq* represents water in pores of Berea sandstone, and *Lpq* and *Spq* represent water in large and small pores of Indiana limestone, respectively. Only the gross features of $I(T_{1,p}, T_{2,q})$ are observed with large regularization parameters. However, with a decrease in the regularization parameter, low-intensity nonground eigenvalues of the diffusion-relaxation system, such as *P*11, *P*22, *L*11, and *S*11 emerge. Therefore, the variation of the regularization term is employed to aid interpretation in magnetic resonance relaxation analysis rather than attempting to choose a single appropriate regularization parameter. *N*0*q* are diffusion-relaxation eigenvalues related to ^{1}H that do not experience the effect of pore walls and demonstrate bulklike behavior in the T_1 domain.

Pearling or peak splitting is another important feature of variation of the regularization parameter in Fig. 2. This is a common feature of algorithms employed in multiexponential analysis [20]. In such cases, a single broad peak may break into smaller peaks, as observed in the case of *P*00 at $\alpha = 0.1$ for the Berea sandstone in Fig. 2. Pearling does not affect the detection of ground and nonground eigenvalues. It only affects the ground eigenvalue peak at small regularization parameters. The T_1, T_2, and intensity of the ground eigenvalue peak are detected at a large regularization parameter, for example at $\alpha = 1000$ in Fig. 2. Even at small regularization parameters, pearling does not change the position of the peak.

Peaks of small amplitude that sometimes appear in erroneous positions in $T_1 - T_2$ data are different from pearling

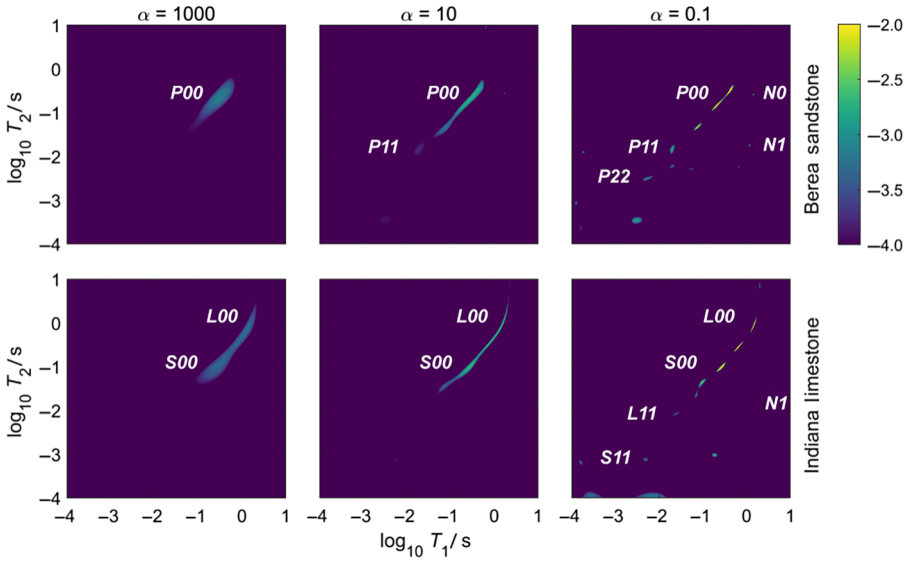

FIG. 2. Two-dimensional relaxation correlation functions $I(T_{1,p}, T_{2,q})$ for brine-saturated Berea sandstone (top) and Indiana limestone (bottom) at $B_0 = 0.05$ T and regularization parameters of $\alpha = 1000$, 10, and 0.1. Intensity range of $10^{-4} - 10^{-2}$ is mapped from purple (black) to yellow (white), respectively, using a logarithmic scale to reveal small eigenvalues. Only ground eigenvalues are visible at $\alpha = 1000$. Nonground eigenvalues emerge at $\alpha = 10$ and 0.1. Wide ground-state peaks split at small regularization parameters [20]. *P*00, *P*11, and *P*22 are the first three eigenvalues of magnetization relaxation in Berea sandstone. In the case of Indiana limestone, *Spq* and *Lpq*, respectively, represent eigenvalues of small and large pores. *N*0*q* marks the signal that demonstrates bulklike features in the T_1 domain.

effects. However, they do not affect our analysis. They may be caused by SNR problems. In laboratory measurements where SNR is usually greater than 100, random peaks rarely appear, and they have very low intensities. The intensity of nonground eigenvalues is greater than any possible random peaks at SNR > 100. Therefore, at least the first nonground eigenvalue will not be buried in noise. The $I(T_{1,p}, T_{2,q})$ data in Fig. 2 is shown in $\log_{10}$-scale of intensity and the range of -4 and -2 for two main reasons: (a) filtering any insignificant low-intensity peaks with $\log_{10} I(T_{1,p}, T_{2,q}) < -4$, while at the same time (b) enhancing the visibility of low-intensity features by using a logarithmic intensity scale.

The procedure for the detection of ground and nonground eigenvalues begins as follows. For normalized time-domain data, the 2D inversion method [17] with a regularization parameter of $\alpha = 1000$ provides sufficient smoothing to only show ground eigenvalues. At $\alpha = 1000$, if there is only one peak, such as the Berea sandstone shown in Fig. 2, the pore size distribution is unimodal. If two peaks exist at $\alpha = 1000$, the pore size distribution is bimodal and the ratio between the integral intensity of peaks is the ratio between their volumetric contributions to porosity. This is the case for the Indiana limestone sample shown in Fig. 2.

The Brownstein-Tarr theory provides guidelines to distinguish nonground eigenvalue peaks relative to the ground peak. A correct combination of l, ρ_1, and ρ_2 leads to a cluster of peaks that, through the Brownstein-Tarr theory, matches experimental peak locations in $T_1 - T_2$ experiments. At small regularization parameters, such as that of $\alpha = 0.1$, nonground eigenvalues emerge as peaks with shorter characteristic times and smaller intensities relative to the ground eigenvalues. The characteristic time of the first nonground eigenvalue is approximately 0.1 of that of the ground eigenvalue and its intensity is $2\% - 10\%$ of that of the ground eigenvalue. The nonground eigenvalues should also meet the condition of $T_2 \leq T_1$ and usually fall on or close to the linear diagonal line of the $T_1 - T_2$ correlation plot. These guidelines aid in the selection of a physically sensible peak as the nonground eigenvalue to be tested with an optimization algorithm based on the Brownstein-Tarr theory. If experimental peaks are not chosen correctly, theory does not match with experimental results and one would know that the chosen nonground eigenvalue peak is not detected correctly. This process can be repeated until a cluster of eigenvalues that satisfactorily matches theory is found.

A direct search optimization method [21] varies $\log_{10} l/\mu$m, $\log_{10}\rho_1/(\mu$m/s), and $\log_{10}\rho_2/(\mu$m/s) and solves Eqs. (7)–(9) for the planar geometry to match the time constants of eigenvalues detected in $I(T_{1,p}, T_{2,q})$. Input parameters are all constrained in the range of $10^{-2} - 10^{-8}$ and have starting values of 10^{-6}, 10^{-4}, and 10^{-4}. Eigenvalues calculated from Eq. (9) are corrected for bulk relaxation of two mass-percent NaCl solution at $B_0 = 0.05$ T, $T_{1b} = 3.07$, and $T_{2b} = 2.80$ s. Within the objective function of the optimization method, the roots of

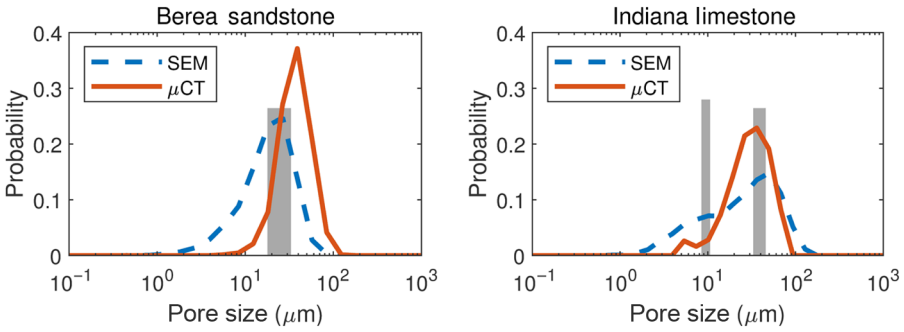

FIG. 3. Volumetric probability of pore diameter from SEM (– –) and x-ray micro tomography (—) for Berea sandstone (left) and Indiana limestone (right). The pore size from magnetic resonance relaxation by a direct search algorithm is shown as a gray rectangle. A pore diameter of 22.1 μm is computed for Berea sandstone and pore diameters of the large and small pores in Indiana limestone are estimated to be 39.6 and 10.0 μm. The width of the rectangle shows the estimated size by varying the input parameters and the heights demonstrate relative pore size population.

$x \cdot \tan x - \mathrm{Da}_i^{\mathrm{II}}$ are computed employing a combination of bisection, secant, and inverse quadratic interpolation methods in the ranges of $(0,\ \pi/2-\varepsilon)$, $(\pi, 3\pi/2-\varepsilon)$, and $(2\pi,\ 5\pi/2-\varepsilon)$, respectively, for the ground, the first nonground, and the second nonground eigenvalues with $\varepsilon = 1\times10^{-16}$.

The optimization method correctly matches the measured eigenvalues with liberal constraints for l, ρ_1, and ρ_2. For Berea sandstone, this work predicts a 22.1-μm pore size; whereas the pore size from SEM and x-ray micro tomography have modes of 26 and 39 μm, respectively, as shown in Fig. 3. Berea sandstone has estimated surface relaxivity constants of $\rho_1 = 138$ and $\rho_2 = 237$ μm/s. The predicted pore size agrees with previously published results for surface-area-to-volume ratio of Berea sandstone [22]. Surface relaxivities of Berea sandstone calculated in this work are less than a factor of 10 different from those reported in the literature [22,23]. With samples used in this study, Eqs. (7)–(9) demonstrate a greater sensitivity to the pore size as opposed to surface relaxivities.

For Indiana limestone, the analytical method presented in this work estimates pore sizes of 10.0 and 39.6 μm for small and large pores, respectively, as shown in Fig. 3. The pore sizes from processed SEM images are 10.1 and 50 μm for small and large pores, respectively. Indiana limestone has estimated surface relaxivity constants of $\rho_1 = 64$ and $\rho_2 = 204$ μm/s for small pores and $\rho_1 = 60$ and $\rho_2 = 195$ μm/s for large pores. Surface relaxivities of large and small pores are satisfactorily similar although they are acquired with two separate sets of eigenvalues. These results agree with previously published results for Indiana limestone pore size [24,25] and surface relaxivity of Indiana limestone is within the expected surface relaxivity range for sedimentary rocks [22].

In all cases studied in this research, observed intensities of the nonground relaxation eigenvalues are slightly larger than those estimated. Brownstein and Tarr calculated the intensity of nonground eigenvalues for planar, cylindrical, and spherical geometries and realized that the contribution of nonground eigenvalues is larger for cylindrical and spherical geometries with the same $\mathrm{Da}_i^{\mathrm{II}}$ values [19]. The majority of the discrepancy between estimated and measured intensities of nonground eigenvalues is due to the simple planar geometry assumed in this work.

$T_1 - T_2$ measurements are performed with a B_0 static magnetic field of 0.05 T and 90° rf pulse lengths of 27 μs. Measurements are undertaken at an ambient temperature of 24 °C. τ_1 is varied logarithmically $P = 56$ times, in the range of 0.1 ms to 15 s, and $N = 8125$ echoes are acquired with $\tau_i = 125$ or 300 μs. Each measurement is repeated four times for signal averaging and phase cycling with a repetition delay of 20 s. The measurement time for sandstone and limestone samples is 106 and 156 min. The inverse integral transform method of [17] converts $m_+(\tau_1,\tau_2)$ to $I(T_{1,p},T_{2,q})$ with $T_{i,p}$ in the range of 1 μs to 10 s in 512 logarithmic steps. Logarithmic variation of the regularization parameter from 100 000 down to 0.01 reduces blurring in $I(T_{1,p},T_{2,q})$ while maintaining the main features of $I(T_{1,p},T_{2,q})$ (see Supplemental Material [26]). The regularization parameter is not reduced beyond 0.01 for normalized m_+ matrices. The SNR of $m_+(\tau_1,\tau_2)$ is 168 and 123 for the Berea sandstone and Indiana limestone samples. Two-dimensional microscopy or three-dimensional microtomography images are corrected by a median filter, binarized with adaptive thresholding [27], and reduced to skeletons [28]. The value of the distance transform at each skeleton voxel is regarded as its respective pore radius. After binning, pore size probabilities are corrected according to their volumetric contribution.

In summary, we demonstrate how uniform magnetization in natural porous media may result in nonground eigenvalues detected by 2D magnetic resonance relaxation measurements. It is also shown that the distinctive pattern of these eigenvalues makes possible identification of

multiple pore sizes with the possibility of further processing to yield the standard deviation of pore size. In the future, we are going to apply this method and its variants to a variety of rocks and other porous materials of technological importance such as wood and cement.

ACKNOWLEDGMENT

Armin Afrough thanks the NBIF, APEGNB of New Brunswick, and UNB School of Graduate Studies. Bruce J. Balcom acknowledges NSERC of Canada for a Research Chair in Material Science MRI. Authors thank Atlantic Innovation Fund, Saudi Aramco, ConocoPhillips, and Green Imaging Technologies for financial support; Steve Cogswell from UNB Microscopy and Microanalysis for microscopy; Zong-Chao Yan for comments; and Compute Canada for computational resources.

[1] D. O. Seevers, in *Proceedings of the Society of Petrophysicists and Well-Log Analysts 7th Annual Logging Symposium*, Tulsa (1966).

[2] Y.-Q. Song, Detection of the High Eigenmodes of Spin Diffusion in Porous Media, Phys. Rev. Lett. **85**, 3878 (2000).

[3] Y.-Q. Song, S. Ryu, and P. N. Sen, Determining multiple length scales in rocks, Nature **406**, 178 (2000).

[4] P. T. Callaghan, A. Coy, D. MacGowan, K. J. Packer, and F. O. Zelaya, diffraction-like effects in NMR diffusion studies of fluids in porous solids, Nature **351**, 467 (1991).

[5] P. T. Callaghan, A. Coy, T. P. J. Halpin, D. MacGowan, K. J. Packer, and F. O. Zelaya, Diffusion in porous systems and the influence of pore morphology in pulsed gradient spin-echo nuclear magnetic resonance studies, J. Chem. Phys. **97**, 651 (1992).

[6] H. C. Torrey, Bloch equations with diffusion terms, Phys. Rev. **104**, 563 (1956).

[7] R. K. Kleinberg, in *Experimental Methods in the Physical Sciences*, edited by P. -Z. Wong (Academic Press, San Diego, 1999), Vol. 35, pp. 337–385.

[8] Y.-Q. Song, L. Zielinski, and S. Ryu, Two-Dimensional NMR of Diffusion Systems, Phys. Rev. Lett. **100**, 248002 (2008).

[9] Y.-Q. Song, G. Carneiro, L. M. Schwartz, and D. L. Johnson, Experimental Identification of Diffusive Coupling Using 2D NMR, Phys. Rev. Lett. **113**, 235503 (2014).

[10] D. L. Johnson and L. M. Schwartz, Analytic theory of two-dimensional NMR in systems with coupled macro- and micropores, Phys. Rev. E **90**, 032407 (2014).

[11] K. Keating, A laboratory study to determine the effect of surface area and bead diameter on NMR relaxation rates of glass bead packs, Near Surf. Geophys. **12**, 243 (2014).

[12] M. Müller-Petke, R. Dlugosch, J. Lehmann-Horn, and M. Ronczka, Nuclear magnetic resonance average pore-size estimations outside the fast-diffusion regime, Geophysics **80**, D195 (2015).

[13] S. Costabel, C. Weidner, M. Müller-Petke, and G. Houben, Hydraulic characterisation of iron oxide-coated sand and gravel based on nuclear magnetic resonance relaxation modes analyses, Hydrol. Earth Syst. Sci. **22**, 1713 (2018).

[14] J. H. Lee, C. Labadie, C. S. Springer, and G. S. Harbison, Two-dimensional inverse laplace transform NMR: Altered relaxation times allow detection of exchange correlation, J. Am. Chem. Soc. **115**, 7761 (1993).

[15] Y.-Q. Song, L. Venkataramanan, M. D. Hürlimann, M. Flaum, P. Frulla, and C. Straley, T_1–T_2 correlation spectra obtained using a fast two-dimensional Laplace inversion, J. Magn. Reson. **154**, 261 (2002).

[16] P. T. Callaghan, C. H. Arns, P. Galvosas, M. Hunter, Y. Qiao, and K. E. Washburn, Recent Fourier and Laplace perspectives for multidimensional NMR in porous media, Magn. Reson. Imaging **25**, 441 (2007).

[17] L. Venkataramanan, Y.-Q. Song, and M. D. Hürlimann, Solving fredholm integrals of the first kind with tensor product structure in 2 and 2.5 dimensions, IEEE Trans. Signal Process. **50**, 1017 (2002).

[18] R. B. Bird, W. E. Stewart, and E. N. Lightfoot, *Transport Phenomena*, 2nd ed. (John Wiley & Sons, New York, 2002), p. 551.

[19] K. R. Brownstein and C. E. Tarr, Importance of classical diffusion in NMR studies of water in biological cells, Phys. Rev. A **19**, 2446 (1979).

[20] G. C. Borgia, R. J. S. Brown, and P. Fantazzini, Uniform-penalty inversion of multiexponential decay data, J. Magn. Reson, **132**, 65 (1998).

[21] T. G. Kolda, R. M. Lewis, and V. Torczon, Optimization by direct search: New perspectives on some classical and modern methods, SIAM Rev. **45**, 385 (2003).

[22] M. D. Hürlimann, K. G. Helmer, L. L. Latour, and C. H. Sotak, Restricted diffusion in sedimentary rocks. Determination of surface-area-to-volume ratio and surface relaxivity, J. Magn. Reson. Ser. A **111**, 169 (1994).

[23] Z.-X. Luo, J. Paulsen, and Y.-Q. Song, Robust determination of surface relaxivity from nuclear magnetic resonance DT_2 measurements, J. Magn. Reson. **259**, 146 (2015).

[24] M. Freire-Gormaly, J. S. Ellis, H. L. MacLean, and A. Bazylak, Pore structure characterization of Indiana limestone and pink dolomite from pore network reconstructions, Oil Gas Sci. Technol. **71**, 33 (2016).

[25] Y. Ji, P. Baud, V. Vajdova, and T.-F. Wong, Characterization of pore geometry of Indiana limestone in relation to mechanical compaction, Oil Gas Sci. Technol. **67**, 753 (2012).

[26] See Supplemental Material at http://link.aps.org/supplemental/10.1103/PhysRevApplied.11.041002 for the effect of variation of the regularization parameter on $I(T_{1,p}, T_{2,q})$ in Berea sandstone and Indiana limestone.

[27] D. Bradley and G. Roth, Adaptive thresholding using the integral image, J. Graph. Tools **12**, 13 (2007).

[28] T. C. Lee, R. L. Kashyap, and C. N. Chu, Building skeleton models via 3-D medial surface axis thinning algorithms, CVGIP Graph. Model. Image Process. **56**, 462 (1994).